

## Mechanistic Basis of the Inhibition of Type II Dehydroquinase by (2*S*)- and (2*R*)-2-Benzyl-3-dehydroquinic Acids

Emilio Lence,<sup>†</sup> Lorena Tizón,<sup>†</sup> José M. Otero,<sup>‡</sup> Antonio Peón,<sup>†</sup> Verónica F. V. Prazeres,<sup>†</sup> Antonio L. Llamas-Saiz,<sup>§</sup> Gavin C. Fox,<sup>||</sup> Mark J. van Raaij,<sup>⊥</sup> Heather Lamb,<sup>¶</sup> Alastair R. Hawkins,<sup>¶</sup> and Concepción González-Bello<sup>\*,†</sup>

<sup>†</sup>Centro Singular de Investigación en Química Biológica y Materiales Moleculares (CIQUS), <sup>‡</sup>Departamento de Bioquímica y Biología Molecular, Facultad de Farmacia, and <sup>§</sup>Unidad de Rayos X, RIAIDT, Edificio CACTUS, Universidad de Santiago de Compostela, 15782 Santiago de Compostela, Spain

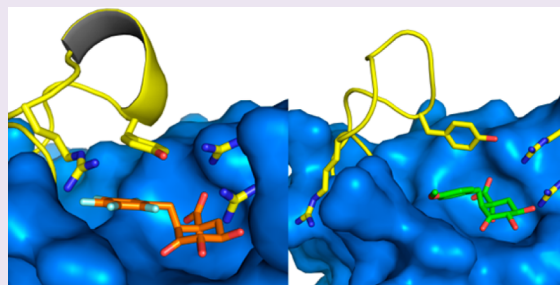
<sup>||</sup>Proxima 2, Synchrotron SOLEIL, L'Orme des Merisiers, Saint-Aubin, F-91192 Gif-sur-Yvette, France

<sup>⊥</sup>Departamento de Estructura de Macromoléculas, Centro Nacional de Biotecnología (CSIC), Campus Cantoblanco, 28049 Madrid, Spain

<sup>¶</sup>Institute of Cell and Molecular Biosciences, Medical School, University of Newcastle upon Tyne, Newcastle upon Tyne NE2 4HH, U.K.

### S Supporting Information

**ABSTRACT:** The structural changes caused by the substitution of the aromatic moiety in (2*S*)-2-benzyl-3-dehydroquinic acids and its epimers in C2 by electron-withdrawing or electron-donating groups in type II dehydroquinase enzyme from *M. tuberculosis* and *H. pylori* has been investigated by structural and computational studies. Both compounds are reversible competitive inhibitors of this enzyme, which is essential in these pathogenic bacteria. The crystal structures of *M. tuberculosis* and *H. pylori* in complex with (2*S*)-2-(4-methoxy)benzyl- and (2*S*)-2-perfluorobenzyl-3-dehydroquinic acids have been solved at 2.0, 2.3, 2.0, and 1.9 Å, respectively. The crystal structure of *M. tuberculosis* in complex with (2*R*)-2-(benzothiophen-5-yl)methyl-3-dehydroquinic acid is also reported at 1.55 Å. These crystal structures reveal key differences in the conformation of the flexible loop of the two enzymes, a difference that depends on the presence of electron-withdrawing or electron-donating groups in the aromatic moiety of the inhibitors. This loop closes over the active site after substrate binding, and its flexibility is essential for the function of the enzyme. These differences have also been investigated by molecular dynamics simulations in an effort to understand the significant inhibition potency differences observed between some of these compounds and also to obtain more information about the possible movements of the loop. These computational studies have also allowed us to identify key structural factors of the *H. pylori* loop that could explain its reduced flexibility in comparison to the *M. tuberculosis* loop, specifically by the formation of a key salt bridge between the side chains of residues Asp18 and Arg20.



In the past few years, our research group has been studying the possible development of new antibiotics by inhibition of the third enzyme of the shikimic acid pathway, dehydroquinase (3-dehydroquinase dehydratase, DHQ, EC 4.2.1.10). In particular, we have focused on the inhibition of two pathogenic bacteria, *Mycobacterium tuberculosis*, the causative agent of tuberculosis, and *Helicobacter pylori*, the causative agent of gastric and duodenal ulcers, which has also been classified as a type I carcinogen. The DHQ enzymes from these bacteria are encoded by the genes *aroD* and *aroQ/aroD*, respectively.<sup>1,2</sup> There are two distinct dehydroquinases, known as type I and type II, which have different biochemical and biophysical properties and exhibit no significant sequence or structural similarity. Both subtypes catalyze the same overall reaction through independent mechanisms and with opposite stereochemistry.<sup>3,4</sup>

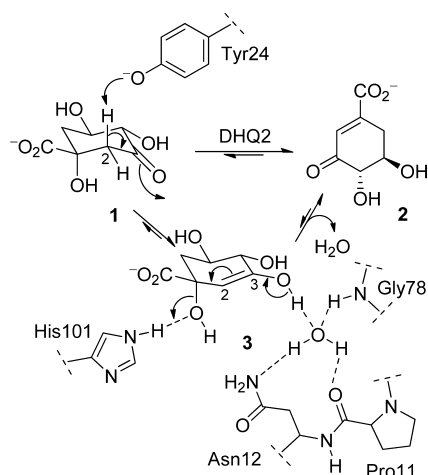
The type II enzyme, which is present in *M. tuberculosis* and *H. pylori*, catalyze the *anti* elimination of water involving the loss of the more acidic pro-*S* hydrogen from C2 of 3-dehydroquinic acid (**1**) to form 3-dehydroshikimic acid (**2**) (Scheme 1).<sup>5,6</sup> Two residues, an arginine (Arg19 and Arg17 in *M. tuberculosis* and *H. pylori*, respectively) and a tyrosine (Tyr24 and Tyr22 in *M. tuberculosis* and *H. pylori*, respectively), have been identified by chemical modification and site-directed mutagenesis studies as being essential for enzyme activity.<sup>7,8</sup> Both residues are located in the flexible loop that closes over the active site upon substrate binding. The elimination proceeds through a stepwise E<sub>1</sub>CB mechanism<sup>5</sup> involving an

Received: September 14, 2012

Accepted: November 30, 2012

Published: November 30, 2012

**Scheme 1. Enzymatic Conversion of 3-Dehydroquinic Acid (1) to 3-Dehydroshikimic Acid (2) Catalyzed by DHQ2<sup>a</sup>**



<sup>a</sup>The reaction proceeds *via* an enol intermediate 3. Relevant residues are indicated (the numbering corresponds to *M. tuberculosis*).

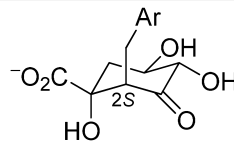
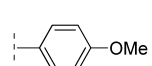
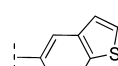
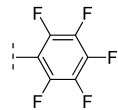
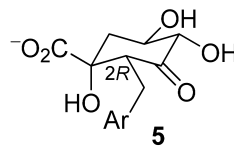
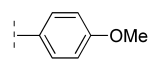
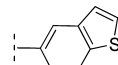
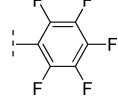
enol intermediate 3, which is stabilized by a conserved water molecule that interacts through hydrogen-bonding with a conserved asparagine (Asn12 and Asn10 in *M. tuberculosis* and *H. pylori*, respectively), the carbonyl group of a conserved proline (Pro11 and Pro9 in *M. tuberculosis* and *H. pylori*, respectively), and the main-chain amide of Gly78 in *M.*

*tuberculosis* or Ala19 in *H. pylori* (Scheme 1).<sup>6</sup> The reaction is initiated by the essential tyrosine, and the final step is the acid-catalyzed elimination of the C1 hydroxyl group, a reaction mediated by a conserved histidine acting as a proton donor.

We have shown previously that the substitution of either the pro-*R* or pro-*S* hydrogen from C2 of 1 by a functionalized benzyl group provides good reversible competitive inhibitors of this enzyme (Table 1).<sup>8</sup> The resolution of the crystal structures of the binary complexes between DHQ2 from *M. tuberculosis* (DHQ2-Mt) and *H. pylori* (DHQ2-Hp) and one of the most potent inhibitors of the 2*R*-substituted derivatives 5, the 4-methoxybenzyl derivative 5a, which has *K<sub>i</sub>* values of 26 nM and 170 nM, respectively, reveal that the essential arginine is expelled from the active site and faces away from the essential tyrosine.<sup>10</sup> Molecular dynamics simulations suggest that the benzyl groups of ligands 5 inactivate the enzyme by causing a significant conformational change in the flexible loop, a change that prevents appropriate orientation of the tyrosine for proton abstraction.<sup>10</sup> It is important to highlight that the 2*R*-substituted derivatives 5 still contain the axial hydrogen that could be removed by the essential tyrosine, the residue that triggers the dehydration reaction.

For the DHQ2-Mt enzyme, the biological results showed that the substitution of either the pro-*R* or pro-*S* hydrogen from C2 of 1 by either an electron-rich or electron-withdrawing benzyl group provides good reversible competitive inhibitors, all of which are in the low nanomolar range (Table 1). For the DHQ2-Hp enzyme, the differences in inhibition potencies

**Table 1. *K<sub>i</sub>* (nM) Values for (2*S*)-4 and (2*R*)-2-Benzyl-3-dehydroquinic Acids 5 against DHQ2-Mt and DHQ2-Hp and PDB Accession Codes<sup>9</sup>**

Compound	Ar	<i>M. tuberculosis</i> <sup>a</sup>		<i>H. pylori</i> <sup>b</sup>	
		<i>K<sub>i</sub></i>	PDB	<i>K<sub>i</sub></i>	PDB
 4	a 	100	4B6O	1420	4B6R
	b 	56	--	900	--
	c 	74	4B6P	970	4B6S
 5	a 	26	2XB8 <sup>10</sup>	170	2XB9 <sup>10</sup>
	b 	28	4B6Q	160	--
	c 	47	--	2600	--

<sup>a</sup>*K<sub>m</sub>* = 15 μM, *k<sub>cat</sub>* = 0.15 s<sup>-1</sup> under assay conditions: Tris-HOAc (50 mM, pH 7.0, 25 °C). <sup>b</sup>*K<sub>m</sub>* = 448 μM, *k<sub>cat</sub>* = 0.06 s<sup>-1</sup> under assay conditions: Tris-HCl (50 mM, pH 7.0, 25 °C).

Table 2. Crystallographic Data Collection and Refinement Statistics for the DHQ2 Complexes with Inhibitors 4a, 4c, and 5b

data processing <sup>a</sup>	DHQ2-Mt/4a	DHQ2-Mt/4c	DHQ2-Mt/5b	DHQ2-Hp/4a	DHQ2-Hp/4c
space group	F23	F23	F23	P4 <sub>2</sub> 22	P4 <sub>2</sub> 22
cell parameters (Å) <sup>b</sup>	<i>a</i> = <i>b</i> = <i>c</i> = 126.19	<i>a</i> = <i>b</i> = <i>c</i> = 126.27	<i>a</i> = <i>b</i> = <i>c</i> = 126.27	<i>a</i> = <i>b</i> = 100.44, <i>c</i> = 104.30	<i>a</i> = <i>b</i> = 100.19, <i>c</i> = 104.58
wavelength (Å)	0.93340	0.98011	0.98011	0.98011	0.98011
detector	ADSC Q210 CCD	ADSC Q315r CCD	ADSC Q315r CCD	ADSC Q315r CCD	ADSC Q315r CCD
measured reflections <sup>c</sup>	11386 (1651) <sup>d</sup>	7534 (1086) <sup>d</sup>	24267 (3515) <sup>d</sup>	36522 (5234) <sup>d</sup>	42501 (6100) <sup>d</sup>
resolution range (Å)	63.1–2.00 (2.11–2.00)	44.6–2.30 (2.43–2.30)	38.0–1.55 (1.63–1.55)	58.7–2.00 (2.11–2.00)	58.7–1.90 (2.00–1.90)
Wilson B (Å <sup>2</sup> )	13.2	27.5	18.8	33.8	25.8
multiplicity	7.4 (7.4)	4.3 (4.3)	6.6 (5.8)	4.4 (3.9)	7.8 (6.8)
completeness	1.000 (1.000)	1.000 (1.000)	0.999 (0.997)	0.997 (1.000)	0.998 (0.999)
<i>R</i> <sub>merge</sub>	0.101 (0.334)	0.113 (0.391)	0.057 (0.381)	0.080 (0.344)	0.062 (0.293)
	Refinement <sup>e</sup>				
resolution range (Å)	38.0–2.00 (2.11–2.00)	44.6–2.30 (2.42–2.30)	38.0–1.55 (1.62–1.55)	58.7–2.00 (2.11–2.00)	58.7–1.90 (2.00–1.90)
reflections used in refinement <sup>d</sup>	10274 (1492)	7144 (1025)	23379 (3387)	34582 (4973)	41125 (6017)
reflections used for <i>R</i> <sub>free</sub>	1104 (151)	1025 (55)	1296 (178)	1876 (248)	1180 (21)
<i>R</i> -factor <sup>f</sup>	0.144 (0.157)	0.169 (0.211)	0.134 (0.176)	0.212 (0.270)	0.226 (0.385)
<i>R</i> <sub>free</sub> <sup>g</sup>	0.178 (0.212)	0.223 (0.312)	0.166 (0.217)	0.276 (0.330)	0.278 (0.415)
rmsd (bonds (Å)/angles (deg))	0.014/1.4	0.015/1.5	0.014/1.6	0.016/1.5	0.014/1.5
	Final Model				
protein/inhibitor/water/solvent atoms	1119/22/136	1096/25/72	1078/23/164	3714/66/184	3675/75/241
average B protein/inhibitor/solvent (Å <sup>2</sup> )	14.2/8.8/28.0	19.7/17.9/27.7	17.9/19.4/36.0	45.4/43.3/47.2	33.0/26.7/37.8
Ramachandran statistics <sup>h</sup> (%)	95.7/98.6	96.4/100.0	98.5/100.0	95.1/99.4	96.1/99.4
PDB accession code	4B6O	4B6P	4B6Q	4B6R	4B6S

<sup>a</sup>Results from SCALA (ref 25). <sup>b</sup>1 Å is 0.1 nm. <sup>c</sup>No  $\sigma$  cutoff or other restrictions were used for inclusion of reflections. <sup>d</sup>Values in parentheses are for the highest resolution bin, where applicable. <sup>e</sup>Results from REFMAC (ref 31). <sup>f</sup> $R$ -factor =  $\sum ||F_{\text{obs}}(hkl)| - |F_{\text{calc}}(hkl)|| / \sum |F_{\text{obs}}(hkl)|$ . <sup>g</sup>According to Brünger (ref 30). <sup>h</sup>According to the program MOLPROBITY (ref 32). The percentages indicated are for residues in favored and total allowed regions, respectively.

between the 2*R*-substituted derivatives **5** and the 2*S*-substituted derivatives **4** are more pronounced, with the 2*R*-substituted derivatives **5** being more potent in general. However, this trend is broken by the pentafluorobenzyl analogue **5c**, which showed a *K*<sub>i</sub> significantly higher (2.6  $\mu$ M) than those of the other 2*R*-substituted derivatives **5a** and **5b** (0.16 and 0.17  $\mu$ M, respectively).

Intrigued by the fact that the substitution of either the pro-*R* or pro-*S* hydrogen from C2 of **1** by either an electron-rich or electron-withdrawing benzyl group provides good reversible competitive inhibitors of these enzymes, in particular for DHQ2-Mt, we decided to gain further insights into the interaction of the 2*S*-substituted derivatives **4** and to analyze the differences in the binding mode of the two series, compounds **4** and **5**. To this end, the crystal structures of both DHQ2 enzymes in complex with two 2*S*-substituted derivatives **4**, the 4-methoxybenzyl derivative **4a**, which has an electron-rich aromatic ring, and the pentafluorobenzyl analogue **4c**, which has an electron-withdrawing aromatic ring, are reported along with the binary complex between DHQ2-Mt and 2*R*-benzothiophen-5-yl derivative **5b**. In addition, the loop conformation differences observed with inhibitors **4a** and **4c** were also studied by molecular dynamics (MD) simulations in order to gain an insight into the role that the type of substituent of the aromatic moiety plays in the binding mode of the inhibitors. Moreover, these MD simulations allowed us to understand the key structural differences responsible for the reduced mobility of the *H. pylori* loop and the significant differences in inhibition potency observed for the 2*R*-

pentafluorobenzyl analogue **5c** between the two DHQ2 enzymes.

## RESULTS AND DISCUSSION

**Structural Studies.** The crystal structures of the 2*S*-4-methoxybenzyl compound **4a** and the 2*S*-pentafluorobenzyl derivative **4c** in complex with DHQ2-Mt and DHQ2-Hp were solved at 2.0, 2.3, 2.0, and 1.9 Å, respectively. In addition, the crystal structure of the binary complex between 2*R*-benzothiophen-5-yl derivative **5b** and DHQ2-Mt was also solved at 1.55 Å. Crystals of the DHQ2-Hp/**5b** complex did not diffract well enough to collect X-ray diffraction data. The binary complexes DHQ2-Hp/**4a**, DHQ2-Hp/**4c**, and DHQ2-Mt/**4c** were obtained by co-crystallization, and the DHQ2-Mt/**4a** and DHQ2-Mt/**5b** binary complex crystals were obtained by soaking apo-DHQ2-Mt<sup>4</sup> crystals. Crystals were flash-frozen directly from the crystallization mixtures by rapid immersion in liquid nitrogen. The crystallization conditions contain enough amount of cryo-protectant (PEG or MPD) to directly freeze the protein crystals in liquid nitrogen without further manipulation. X-ray diffraction data were collected from crystals cryo-cooled in a stream of cold nitrogen gas (100 K) at ambient pressure using synchrotron radiation and were processed. All structures were determined by molecular replacement. For the *H. pylori* enzyme, the crystal structure of DHQ2-Hp bound to citrate described by Laphorn *et al.* (PDB code: 2C4V<sup>11</sup>) was used as a search model and was refined. For the *M. tuberculosis* enzyme, the crystal structure of DHQ2-Mt bound to 3-hydroxyimino quinic acid (PDB code: 1H0S)<sup>12</sup> was employed.

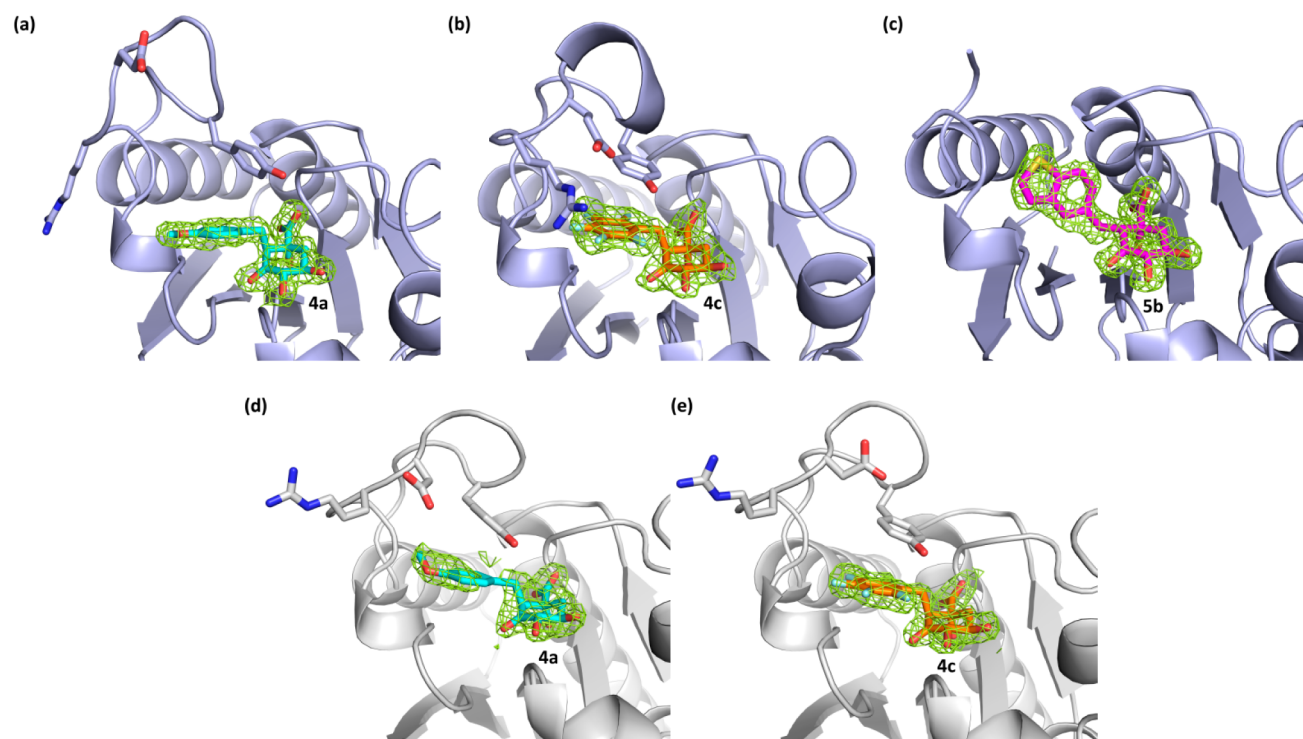


**Figure 1.** Unbiased electron density for inhibitors in a binary complex: (a) DHQ-Mt/4a (PDB code: 4B6O); (b) DHQ-Mt/4c (PDB code: 4B6P); (c) DHQ-Mt/5b (PDB code: 4B6Q); (d) DHQ-Hp/4a (chain A, PDB code: 4B6R); (e) DHQ-Hp/4c (chain A, PDB code: 4B6S). From the model obtained by molecular replacement and before inclusion of the inhibitor molecule, refinement was performed to obtain unbiased density for the inhibitor molecule and other model changes. A maximum-likelihood weighted  $2F_o - F_c$  map contoured at  $1\sigma$  is shown up to  $1.6 \text{ \AA}$  around the inhibitor molecule (green). The final model [DHQ-Mt (blue); DHQ-Hp (gray)], including the inhibitor molecule [4a (cyan); 4c (orange); 5b (magenta)], is superposed onto the map. The loop is disordered in PDB entry 4B6Q.

A summary of the statistics following data reduction and processing is given in Table 2.

The binary complexes DHQ2-Mt/4a, DHQ2-Mt/4c, and DHQ2-Mt/5b contain a single DHQ2-Mt molecule in the crystallographic asymmetric unit (Figures 1a–c), while DHQ2-Hp/4a and DHQ2-Hp/4c complexes crystallized with three nearly identical copies of the inhibitor-protein complex in the asymmetric unit (with rmsd between the protein  $\alpha$  carbons  $<0.4 \text{ \AA}$ ) (designated molecules A, B, and C, Figures 1d–e).

All structures refine with good geometric parameters, and clear electron density is visible for all amino acids with the exception of those of the very C-terminal amino acids of the *H. pylori* protein and certain residues of the flexible substrate-covering loop of all five structures. The flexibility of this loop is essential for the function of the enzyme, and therefore the presence in the crystals of some disorder in this loop is not surprising. Nevertheless, we were able to model the loop completely in four of the five structures, with the exception being that of the DHQ2-Mt/5b binary complex (Figure 1c). We used these modeled conformations in molecular dynamics simulation studies to obtain further information about the possible movements of the loop (see below).

**1. DHQ2-Mt/4a Binary Complex.** Comparison of this crystal structure with our solved crystal structure for DHQ2-Mt in complex with its epimer on C2, *i.e.*, compound 5a (PDB code: 2XB8<sup>10</sup>), shows that both structures are virtually identical ( $0.8 \text{ \AA}$  root-mean-square difference for C- $\alpha$  atoms after superposition) with the exception of the loop that closes over the active site upon substrate binding (see Supporting Information). In the crystal structure reported here, the loop conformation changes significantly: it moves up by  $4.5 \text{ \AA}$  in

relation to its position in the DHQ2-Mt/5a binary complex to give a more open conformation. This displacement is caused by the axial benzyl group of compound 4a, which prevents the appropriate approach of the essential Tyr24 of the loop to the conserved Arg108 of the active site, a residue that has a significant effect on lowering the  $pK_a$  of Tyr24.<sup>6,10</sup> In this more open conformation of the loop, there is room for the side chain of the essential Arg19 to point toward the active site. Although the electron density is not completely conclusive, we modeled the side chain of Arg19 to point inward with the guanidine group located approximately  $6 \text{ \AA}$  from Tyr24. This situation is in contrast to the epimer, compound 5a, where the Arg19 side chain is expelled from the active site. In addition, a  $\pi$ - $\pi$  stacking interaction between the aromatic rings of Tyr24 and ligand 4a is not observed, but this interaction is evident for its epimer. The axial disposition of the benzyl group of C2 prevents its location in the vicinity of the conserved residues Leu13 and Leu16, as observed for its isomer compound 5a. The benzyl group is therefore displaced away from this apolar pocket of DHQ2 and is located in an intermediate subpocket close to the carbon side chain of Arg15 and Asn12, a region that has been identified as important for the design and efficacy of inhibitors.<sup>13</sup>

**2. DHQ2-Mt/4c Binary Complex.** With the exception of the two poorly ordered amino acids located on the loop, Arg19 and Glu20, this crystal structure is virtually identical to our recently solved crystal structure of DHQ2-Mt in complex with compound 5a (PDB code: 2XB8<sup>10</sup>) ( $0.4 \text{ \AA}$  root-mean-square difference for C- $\alpha$  atoms after superposition) (see Supporting Information). In the structure reported here, the catalytic Tyr24 is stabilized by a set of favorable hydrogen-bonding



interactions with Arg108 and possibly with Glu20 (Figure 2). The main differences in the ligand binding are in the position of

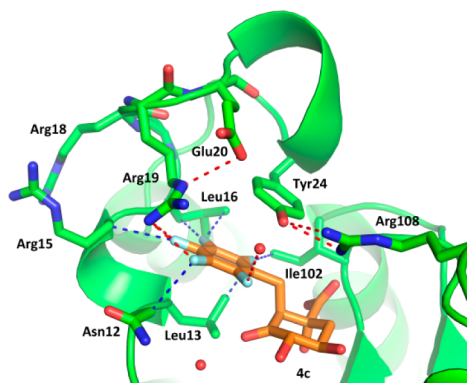


**Figure 2.** Relevant binding interactions of the perfluorobenzyl moiety of inhibitor **4c** in the enzyme–inhibitor crystal structure of DHQ2-Mt (PDB code: 4B6P). Hydrogen-bonding interactions and apolar contacts are shown as red and as blue dashes, respectively.

the benzylic side chain. In this case, the perfluorobenzyl moiety of **4c** establishes an offset  $\pi$ – $\pi$  stacking interaction with the side chain of Tyr24. The guanidinium group of Arg19 has been modeled into density near to the perfluorobenzyl moiety of **4c**, which may form a favorable electrostatic interaction. Moreover, the perfluorobenzyl moiety has a series of  $C_{\text{aryl}}\text{--F}\cdots\text{H}\text{--C}$  attractive contacts with the side chains of Leu13, Leu16, and Ile102 and the carbon side chain of Arg15 and Asn12 (3.3–3.9 Å, see also Supporting Information). Few examples of  $\pi$ – $\pi$  stacking interactions between perfluorophenyl moieties and the aromatic ring of phenylalanine or tyrosine residues have been reported.<sup>14–16</sup>

Two relevant water molecules are shown in the active site (Figure 2). One of them is the essential water molecule involved in the catalytic mechanism, and this forms a hydrogen bond with the carbonyl group of **4c**. The second water molecule interacts through hydrogen-bonding with one of the fluorine atoms of the perfluorobenzyl moiety of **4c** and also with the side chain of Arg108, Arg112, and Asp88 of the neighboring subunit (not shown).

Comparison of the crystal structures of DHQ2-Mt/**4a** and DHQ2-Mt/**4c** binary complexes shows that the binding modes of ligands **4a** and **4c** are quite similar (see Supporting Information), but the different substitution of the aromatic moiety causes different conformational changes of the loop. In both cases, a disruption in the appropriate conformation of the loop for catalysis is obtained, which might explain their similar inhibition constants ( $K_i$  of 100 and 74 nM, respectively). The electron-deficient benzyl group of ligand **4c** is responsible for a strong  $\pi$ – $\pi$  stacking interaction with Tyr24 and a possible favorable electrostatic interaction with the guanidinium group of Arg19. These attractive interactions favor a stable closed form of the loop, the flexibility of which is clearly reduced. These two attractive interactions are not present in binding ligand **4a**, which has an electron-rich aromatic ring. Thus, the 4-methoxybenzyl moiety prevents the approach of Tyr24 for proton abstraction and a more open conformation of the loop is preferred.

**3. DHQ2-Mt/5b Binary Complex.** In this crystal structure, seven amino acids located on the loop (residues 19–25) are not visible. Calculated maps showed clear high electron density

for the inhibitor molecule **5b** (Figure 1c), indicating that the benzothiophenyl group is located approximately perpendicular to the cyclohexane ring and with its sulfur atom orientated toward the flexible loop. In the crystal structure reported here, the benzothiophenyl ring rotates by about  $43^\circ$  toward the tyrosine of the loop and causes a change in the orientation of the side chain of Leu16 (see Supporting Information). This shift allows the establishment of CH– $\pi$  interactions between the side chain of Leu16 and the benzothiophenyl ring, which is more electron-rich than the 4-methoxyphenyl one. With the benzothiophenyl ring located approximately perpendicular to the cyclohexane ring, the closure of the active site is avoided by preventing hydrogen-bonding interaction between the essential Tyr24 and Arg108.

**4. DHQ2-Hp/4a Binary Complex.** As for compound **5a**, the essential Arg17 is expelled from the active site to face away from Tyr22. Surprisingly, despite the axial disposition of the 4-methoxybenzyl group of ligand **4a**, only a small shift of the loop ( $\sim 1.0$  Å) is observed. In fact, the position of ligand **4a** is slightly offset in relation to **5a** in order to accommodate the 4-methoxybenzyl moiety within the active site without altering the loop conformation. We modeled the side chain of Tyr22 in density parallel to the benzyl group of the inhibitor. The results suggest that for the DHQ2-Hp enzyme, the disposition of the essential Tyr22 is preferred when the essential Arg17 is either outside the active site or is too far away to interact with Tyr22. This finding supports the idea that the essential arginine of the loop has a crucial role in the control of the appropriate orientation of the essential tyrosine for proton abstraction.<sup>10</sup>

**5. DHQ2-Hp/4c Binary Complex.** As for ligands **4a** and **5a**, the essential Arg17 appears to point away from the active site, and the perfluorobenzyl group of **4c** interacts by  $\pi$ – $\pi$  stacking (parallel-displaced) with the essential Tyr22 (Figure 3). The

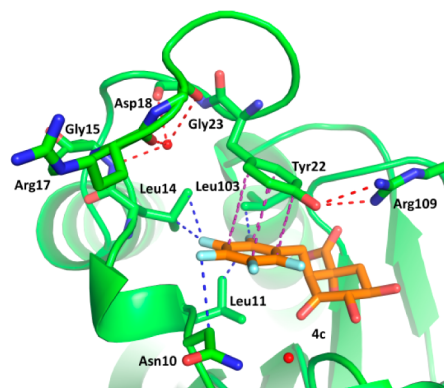


**Figure 3.** Relevant binding interactions of the benzyl moiety of inhibitor **4c** in the enzyme–inhibitor crystal structure of DHQ2-Hp (PDB code: 4B6S). Hydrogen-bonding interactions (red),  $\pi$ – $\pi$  interactions (magenta), and apolar contacts (blue) are indicated as dashes.

loop is slightly more closed than for ligand **4a** ( $\sim 1.4$  Å). The perfluorobenzyl group of **4c** shows several favorable hydrogen-bonding interactions with three nearby bound water molecules (W22, W69, and W230). In addition, a series of  $C_{\text{aryl}}\text{--F}\cdots\text{H}\text{--C}$  attractive contacts with the side chains of Leu11, Leu14, and Leu103 and the carbon side chain of Asn10 are apparent (3.1–3.6 Å, see also Supporting Information).

The structural studies reported here still leave some unresolved issues with regard to the binding mode of **2S-2-**

benzyl derivatives **4**. The 2*S*-2-perfluorobenzyl derivative **4c** seems to close completely the active site of the DHQ2-Mt enzyme with the side chains of Tyr24 and Arg19 inside of the active site. However, this does not seem to occur for the DHQ2-Hp enzyme. Moreover, the binding mode of the 2*S*-4-methoxybenzyl derivative **4a** in the active site of the DHQ2-Hp is similar to that of its epimer **5a**, although they show about 10-fold differences in inhibition constant that are not found for the DHQ2-Mt enzyme. In addition, 2*R*-2-perfluorobenzyl derivative **5c** shows a significantly higher  $K_i$  (2.6  $\mu\text{M}$ ) against the DHQ2-Hp enzyme in comparison to the other components of the series (0.16–0.17  $\mu\text{M}$ ), a situation that does not occur for the *M. tuberculosis* enzyme. We considered that the reasons for some of these differences could be found in the different flexibility of the two loops. In order to gain an insight into these unanswered questions, we decided to carry out a further analysis of the dynamic behavior of the binding mode of these inhibitors in the active site of the DHQ2 by MD simulations studies.

**Molecular Dynamics Simulations Studies.** In order to analyze the relevance of the potential electrostatic interaction observed in the DHQ2-Mt/**4c** binary complex (PDB code: 4B6P) between Arg19 and the perfluorobenzyl moiety of **4c** and to understand why the same behavior is not observed in the binary complex with the DHQ2-Hp enzyme, MD simulations were carried out. First, the DHQ2-Mt/**4c** binary complex was subjected to 10 ns of simulation in order to analyze the dynamic behavior of its  $\pi$ - $\pi$  stacking and potential electrostatic interaction with Tyr24 and Arg19, respectively. Moreover, starting from the DHQ2-Mt/**4c** complex, ligand **4c** was replaced by **4a**, which has an electron-rich ring, and the final complex was submitted to 10 ns of simulation in order to analyze the dynamic behavior of this ligand replacement. Finally, a similar study was performed for the DHQ2-Hp enzyme using the PDB entry 4B6S, which is reported here.

The results for the DHQ2-Mt enzyme show that the relative position of ligand **4c**, Arg19 and Tyr24 in the active site does not change significantly during the simulation (10 ns), suggesting that the interactions of the perfluorobenzyl moiety of **4c** with the guanidinium group of Arg19 (electrostatic) and with the aromatic ring of Tyr24 ( $\pi$ - $\pi$  stacking) are very strong and provide a very stable closed form of the loop. In fact, replacement of the perfluorobenzyl group by a 4-methoxybenzyl one causes, after approximately 1 ns of dynamic simulation, the displacement of the Arg19 side chain from the active site ( $\sim 3$  Å), while the side chain of Tyr24 remains reasonably close to the 4-methoxybenzyl moiety (see Supporting Information).

An attempt by the side chain of Arg17 to enter into the active site was not observed in the MD simulations carried out with the binary complex DHQ2-Hp/**4c**. Moreover, the key  $\pi$ - $\pi$  stacking interaction between the perfluorobenzyl group and the Tyr22 was maintained during the simulation, which shows once again the relevance of this interaction in the binding mode of ligand **4c** in both enzymes. This key  $\pi$ - $\pi$  stacking interaction is easily lost by replacement of the perfluorobenzyl group by a 4-methoxybenzyl one. Thus, after approximately 3 ns of dynamic simulation, the aromatic ring of Tyr22 is clearly displaced away from the 4-methoxybenzyl group, which could explain the lower inhibition potency of ligand **4a** in comparison to ligand **4c** (Figure 4). A more detailed analysis of the dynamic behavior of the loops of both enzymes allowed us to identify structural differences between the two loops that might explain the

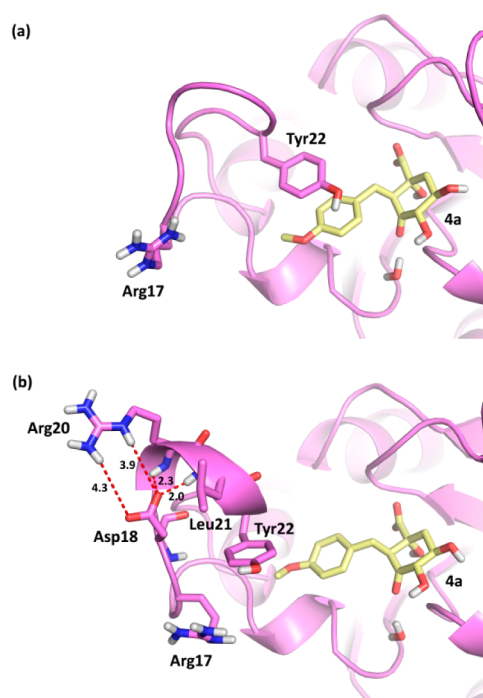


**Figure 4.** Binding mode of ligand **4a** (yellow) in the active site of DHQ2-Hp obtained by MD simulations: (a) after minimization and prior to simulation; (b) after 10 ns of MD. Simulations were carried out using the enzyme geometries found in the crystal structure of DHQ2-Hp/**4c** binary complex (PDB code: 4B6S). Hydrogen-bonding interaction between several residues of the loop is highlighted. Relevant side chain residues are shown and labeled.

different binding mode of ligands **4** in the active site of both enzymes and the differences in their inhibition potency. It was found that the presence of a polar amino acid in the middle of the loop of the *H. pylori* enzyme, specifically Arg20, favors its organization by forming a set of attractive hydrogen bonds that reduces the flexibility of the loop. Such behavior was not observed for the DHQ2-Mt enzyme, which has an alanine in this position (see Supporting Information). These findings are more clearly shown in the dynamic simulation studies carried out with ligand **5c**, which will be discussed below.

**Loop Flexibility and Movement Differences.** Using the enzyme geometries found in the crystal structures of compound **4c** with both enzymes, the binding mode of 2*R*-perfluorobenzyl derivative **5c** was studied. For the DHQ2-Mt enzyme, these studies suggest that the loop would adopt a similar conformation as for ligand **4c**. Thus, the perfluorobenzyl moiety would act as a bridge between the two essential residues, Tyr24 and Arg19, by establishing  $\pi$ - $\pi$  stacking and electrostatic interactions, respectively. In contrast, for the *H. pylori* enzyme, after 1 ns of dynamic simulation a  $\pi$ - $\pi$  stacking interaction with the essential Tyr22 was not observed. In contrast, the loop quickly adopts an open conformation that allows the rotation of the perfluorobenzyl group ( $\sim 90^\circ$ ), which is now approximately perpendicular to the cyclohexane ring. It was observed that the conformation of the loop is clearly controlled by the formation of a key salt bridge between the side chains of residues Asp18 and Arg20 that, once formed, is maintained throughout the simulation period (Figure 5). Similar behavior was also observed in the simulation studies performed with ligand **4a** (see above), although for ligand **5c** it is clearly more pronounced considering the salt bridge

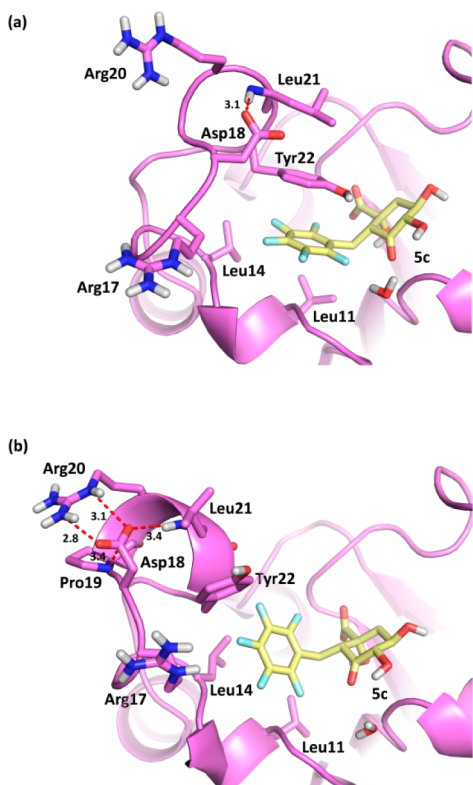


**Figure 5.** Binding mode of ligand **5c** in the active site of DHQ2-Hp (violet) obtained by MD simulations: (a) after minimization and prior to simulation; (b) after 10 ns of MD. Hydrogen-bonding interactions involving residues 18–21 are highlighted. Relevant side chain residues are shown and labeled.

distances, which in this case are 2.8–3.1 Å. The formation of a salt bridge between Asp18 and Arg20, together with the hydrogen bonds between the amide nitrogen of Pro19 and Leu21, might contribute significantly to reduce the mobility of the *H. pylori* loop and to control its movement. In fact, analysis of the amino acid sequence in various DHQ2 (see Supporting Information) reveals that the equivalent residues in the DHQ2-Mt enzyme are Glu20 and Ala22. The *M. tuberculosis* enzyme is the only DHQ2 that has a nonpolar residue in this position, specifically Ala22, which prevents the formation of a similar salt bridge. For the *H. pylori* enzyme, the formation of the salt bridge between Asp18 and Arg20 also appears to promote the electrostatic interaction between the two essential residues of the loop, Arg17 and Tyr22, which remain close once formed (see Supporting Information). The latter interaction could also reduce the electron density of the phenol ring, and therefore the possible  $\pi$ – $\pi$  stacking interaction between the aromatic moiety of the ligand and the aromatic ring of Tyr22 residue would be weaker. This finding supports the idea that the essential arginine of the loop has also a crucial role in controlling the position and the appropriate orientation of Tyr22 residue.

In contrast, the MD simulation studies carried out on the *M. tuberculosis* enzyme showed that the movement of the tyrosine side chain is not controlled by the essential arginine (see Supporting Information). Instead, its position could be mainly controlled by the interaction with the aromatic moiety of the ligand that for the perfluorobenzyl substrate analogues would be a  $\pi$ – $\pi$  stacking one. This is also favored by a greater flexibility of the DHQ2-Mt loop that allows the tyrosine side

chain to be closer to C2 of the substrate analogues. It is probable that, for the *H. pylori* enzyme, the formation of this salt bridge reduces the ability of its loop to accommodate the substituent present on C2 of the substrate analogues **4**. As a consequence, changes to the benzyl group on C2 should have more pronounced effects on their corresponding inhibition potencies than for the DHQ2-Mt enzyme, as experimentally observed.

The MD simulation studies also reveal significant changes in the interaction of ligand **5c** in the active site of DHQ2-Hp with the conserved water involved in the enzymatic mechanism. Only for ligand **5c**, the hydrogen-bonding interaction between its ketone group and the water molecule is lost during the simulation because the position relative to the catalytic water increases (see Supporting Information). As a consequence, the water molecule rotates by approximately 90° and is displaced toward the carbonyl group of Pro9 and the main-chain amide of Ala19. We recently showed that this hydrogen-bonding interaction makes an important contribution to the inhibition potency of mimics of the enol intermediate **3**.<sup>17</sup> We believe that this may also be the case for ligand **5c**.

**Conclusions and Final Remarks.** The structural changes caused by the substitution of the aromatic moiety in (2*S*)-2-benzyl-3-dehydroquinic acids **4** and its epimers **5** by electron-withdrawing or electron-donating groups in type II dehydroquinase enzyme from *M. tuberculosis* and *H. pylori* has been investigated by structural and computational studies.

The crystal structures of *M. tuberculosis* and *H. pylori* in complex with 2*S*-4-methoxybenzyl **4a** and 2*S*-perfluorobenzyl derivatives **4c** have been solved at 2.0, 2.3, 2.0, and 1.9 Å, respectively. The crystal structure of *M. tuberculosis* in complex with 2*R*-benzothiophenyl derivative **5b** is also reported at 1.55 Å. The structural studies reported here show that, for the DHQ2-Hp enzyme and regardless of the type of substituent of the aromatic ring, the binding mode of the 2*S*-2-benzyl derivatives **4** is quite similar, which could explain the similar inhibition constants obtained. In both cases, the essential Arg17, which is located on the loop that closes over the active site upon substrate binding, is expelled from the active site and faces away from the essential Tyr22, the residue that triggers the dehydration reaction. The essential arginine is presumed to orient the tyrosine in an appropriate manner for proton abstraction. In contrast, for the DHQ2-Mt enzyme there are significant differences in the binding mode of these compounds **4** depending on the type of substituent of the aromatic ring, which mainly controls the position of the two essential residues located on the loop. In both compounds **4a** and **4c** there is a dramatic reduction of the loop flexibility, albeit by a different mechanism. Thus, the perfluorobenzyl derivative **4c** causes the complete closure of the active site through the formation of a strong  $\pi$ – $\pi$  stacking interaction with the aromatic ring of Tyr24. In contrast, the 4-methoxybenzyl derivative **4a** favors a more open conformation of the loop, with Arg19 facing out of the active site.

The dynamic behavior of both loops in binding 2*S*-2-benzyl derivatives **4** and their epimers, compounds **5**, were investigated by MD simulations, and this provided an understanding of the reduced mobility of the *H. pylori* loop. For the DHQ2-Mt enzyme, these studies suggest that the perfluorobenzyl moiety of **4c** and its epimer **5c** would act as a bridge between the two essential residues of the loop, Arg19 and Tyr24, through the establishment of strong electrostatic interactions between its fluorine atoms and the guanidinium group of Arg19 and by



strong  $\pi$ - $\pi$  stacking interactions with the aromatic ring of Tyr24. As a consequence, this perfluorobenzyl moiety does not block the entrance of the side chain of the arginine in the active site, as in previously reported PDB entry 2XB8<sup>10</sup> containing 2S-4-methoxybenzyl compound **5a** in the active site, *i.e.*, a ligand with an electron-rich aromatic ring. In addition, the results allowed us to identify key structural differences between the loops of the two enzymes. Specifically, the formation of a salt bridge between Asp18 and Arg20 together with the hydrogen bonds between the amide nitrogen of Pro19 and Leu21 in the DHQ2-Hp enzyme seems to contribute significantly to reducing the mobility of the *H. pylori* loop and to control its movement. The latter interactions could also allow the essential arginine to control the position and the orientation of the tyrosine side chain, which is not observed with the DHQ2-Mt enzyme. This fact could explain, for instance, the significantly higher inhibition constant of the pentafluorobenzyl analogue **5c** against DHQ2-Hp in comparison to the other compounds in these series. For the *M. tuberculosis* enzyme, the MD simulations studies suggest that the movement and the higher flexibility of the loop allow the tyrosine side chain to freely interact with the aromatic moiety of inhibitors **4** and **5**. For compounds substituted with electron-withdrawing groups, a closed conformation of the DHQ2-Mt loop is favored by establishing  $\pi$ - $\pi$  stacking and electrostatic interactions with Tyr24 and Arg19, respectively. The latter is more difficult with the DHQ2-Hp enzyme due to the reduced mobility of its loop and to the interaction between Arg17 and Tyr22. For both enzymes, the aromatic moiety of those inhibitors **4** and **5** substituted with electron-donating groups block the entrance of the essential arginine side chain into the active site. These loop flexibility differences should make the DHQ2-Hp enzyme particularly sensitive to changes introduced in C2 of the natural substrate, because the loop should be less able to accommodate these changes than for the *M. tuberculosis* enzyme, differences that should be considered for future designs.

## METHODS

**Dehydroquinase Assays.** Both enzymes were purified as described previously.<sup>18,19</sup> Concentrated solutions of DHQ2-Hp (6.4 mg mL<sup>-1</sup>) or DHQ2-Mt (2.4 mg mL<sup>-1</sup>) were stored in potassium phosphate buffer (50 mM, pH 7.2), DTT (1 mM), and NaCl (150 mM). When required for assays, aliquots of the enzyme stocks were diluted into water and buffer and stored on ice. Dehydroquinase was assayed in the forward direction by monitoring the increase in absorbance at 234 nm in the UV spectrum due to the absorbance of the enone-carboxylate chromophore of 3-dehydroshikimic acid (**2**) ( $\epsilon/M^{-1} \text{ cm}^{-1}$  12,000). Standard assay conditions were pH 7.0 at 25 °C in Tris-HCl (50 mM) for DHQ2-Hp and Tris-HOAc (50 mM) for DHQ2-Mt. Each assay was initiated by addition of the substrate. Solutions of 3-dehydroquinic acid (**1**) were calibrated by equilibration with DHQ2 and measurement of the change in the UV absorbance at 234 nm due to the formation of the enone-carboxylate chromophore of 3-dehydroshikimic acid (**2**). The  $K_i$  values of acids **4** and **5** against DHQ2 were obtained from Dixon plots ( $1/\nu$  vs  $[I]$ ) of assay data. The initial rates at fixed enzyme and substrate concentrations (0.25–1.4  $K_m$ ) were measured in the absence and in the presence of various inhibitor concentrations.

**Crystallization of DHQ2-Hp/4a, DHQ2-Hp/4c, and DHQ2-Mt/4c Binary Complexes.** Solutions of freshly purified DHQ2-Hp and DHQ2-Mt were concentrated to 20 mg mL<sup>-1</sup> in 50 mM Tris-HCl pH 7.5, 1 mM 2-mercaptoethanol, 1 mM ethylenediaminetetraacetic acid (EDTA) and 200 mM sodium chloride. Compounds **4a** and **4c** were dissolved at 0.25 M in methanol and added at a ratio of 1:20 (v/v) to aliquots of the concentrated protein solution to give solutions of approximately 10 equiv of inhibitor per protein monomer. Diamond-

shaped crystals of up to 0.2 mm  $\times$  0.2 mm of DHQ2-Hp/**4a**, DHQ2-Hp/**4c**, and DHQ2-Mt/**4c** complexes were obtained after 1 month of vapor diffusion in sitting drops composed of 2.0  $\mu$ L of protein/inhibitor solution mixed with 2.0  $\mu$ L of reservoir solution equilibrated against 0.15 mL reservoirs containing 36% (w/v) poly(ethylene glycol) 4000 and 0.1 M sodium citrate pH 5.4, 32% (w/v) poly(ethylene glycol) 4000 and 0.1 M sodium citrate pH 5.4, and 20% (w/v) poly(ethylene glycol) 2000ME and 0.1 M 3-(*N*-morpholino)propanesulfonic acid (MOPS) pH 6.5, respectively.

**Crystallization of DHQ2-Mt/4a and DHQ2-Mt/5b Binary Complexes.** Apo-DHQ2-Mt crystals<sup>4</sup> were soaked in 10 mM solutions of inhibitors **4a** or **5b** in the crystallization mixture [32% (v/v) 2-methyl-2,4-pentenediol, 0.3 M ammonium sulfate, and 0.1 M 4-(2-hydroxyethyl)-piperazine-1-ethanesulfonic acid sodium salt (HEPES sodium salt), pH 7.5] for 24 h.

**Structure Determination of Binary Complexes.** Crystals were flash-frozen directly from the crystallization mixtures by rapid immersion in liquid nitrogen. X-ray diffraction data for DHQ2-Mt/**4a** complex were collected on beamline ID14-1 (ESRF, Grenoble, France) and for DHQ2-Hp/**4a** and **4c** complexes, and DHQ2-Mt/**5b** and **4c** complexes were collected on beamline Proxima 1 (Synchrotron Soleil, Gif-sur-Yvette, France) from crystals maintained at 100 K. The data were processed, scaled, and analyzed using MOSFLM,<sup>20</sup> SCALA,<sup>21</sup> and other programs within the CCP4 software suite.<sup>22</sup> The structures of DHQ2-Hp/**4a** and DHQ2-Hp/**4c** binary complexes were solved by molecular replacement, using the program PHASER<sup>23</sup> with a search model generated from PDB entry 2C4V.<sup>11</sup> Similarly, PDB entry 1H0S<sup>12</sup> was used for DHQ2-Mt binary complexes. Inhibitors' structures and geometrical restraints were generated with the PRODRG server<sup>24</sup> and were manually placed during the model building, which was performed with COOT.<sup>25</sup> Reflections for calculating  $R_{\text{free}}$ <sup>26</sup> were selected in thin shells for DHQ2-Hp/**4a** and DHQ2-Hp/**4c** data and randomly for DHQ2-Mt/**5b**, DHQ2-Mt/**4a**, and DHQ2-Mt/**4c** data. Refinement of the model was performed with REFMAC,<sup>27</sup> and final structure validation was performed with MOLPROBITY.<sup>28</sup> The data collection, refinement and model statistics are summarized in Table 2. Structure figures were prepared using PYMOL.<sup>29</sup>

**Molecular Dynamics Simulations. Ligand Minimization.** Ligand geometries were optimized using a restricted Hartree-Fock (RHF) method and a 6-31G(d) basis set, as implemented in the *ab initio* program Gaussian 09.<sup>30</sup> The resulting wave functions were used to calculate electrostatic potential-derived (ESP) charges employing the restrained electrostatic potential (RESP)<sup>31</sup> methodology, as implemented in the assisted model building with energy refinement (AMBER)<sup>32</sup> suite of programs. The missing bonded and nonbonded parameters were assigned, by analogy or through interpolation from those already present in the AMBER database (GAFF).<sup>30,33</sup>

**Generation and Minimization of the DHQ2-Ligand Complexes.** Simulations were carried out using the enzyme geometries found in the crystal structure of the binary complexes DHQ2-Mt/**4c** (PDB code: 4B6P) and DHQ2-Hp/**4c** (PDB code: 4B6S). Taking into account that unfolding and refolding studies of DHQ2 have shown that the trimer<sup>34</sup> is the biological unit of the enzyme and on the basis of preliminary simulations on the monomer proving to be unstable under our simulation conditions, the trimer was used for these studies. Hydrogens were added to the protein using the web-based PROPKA3.1 server,<sup>35–38</sup> which assigned protonation states to all titratable residues at the chosen pH of 7.0. However,  $\delta$  and/or  $\epsilon$  protonation was manually corrected for His102 (dual) of the active site due to mechanistic considerations and on the basis of results from preliminary MD simulations. Molecular mechanics parameters from the ff03 and GAFF force fields, respectively, were assigned to the protein and the ligands using the LEaP module of AMBER 10.0.<sup>39</sup> All terminal hydrogens were first minimized in vacuum (2000 steps, half of them steepest descent, the other half conjugate gradient). Energy minimization was carried out in two stages using the implicit solvent GB model: first protein side chains (2000 steps, half of them steepest descent, the other half conjugate gradient) and second the entire complex (2000 steps, idem). Thereafter each refined DHQ2-ligand



complex was neutralized by addition of sodium ions and immersed in a truncated octahedron of TIP3P water molecules (10 Å radius).<sup>39–41</sup>

**Simulations.** MD simulations were performed using the AMBER 10.0 suite of programs and Amber ff03 force field. Periodic boundary conditions were applied and electrostatic interactions were treated using the smooth particle mesh Ewald method (PME)<sup>42</sup> with a grid spacing of 1 Å. The cutoff distance for the nonbonded interactions was 9 Å. The SHAKE algorithm<sup>43</sup> was applied to all bonds containing hydrogen, using a tolerance of  $10^{-5}$  Å and an integration step of 2.0 fs. Minimization was carried out in three steps, starting with the octahedron water hydrogens, followed by solvent molecules and sodium counterions and finally the entire system. The minimized system was heated at 300 K (1 atm, 25 ps, a positional restraint force constant of 50 kcal mol<sup>-1</sup> Å<sup>-2</sup>). These initial harmonic restraints were gradually reduced to 5 kcal mol<sup>-1</sup> Å<sup>-2</sup> (10 steps), and the resulting systems were allowed to equilibrate further. MD were carried out for 10 ns. System coordinates were collected every 20 ps for further analysis. A slow-cooling MD simulation was then performed (6 steps until 273 K, 0.2 ns each). Finally, minimization of the entire complexes was performed (100,000 steps, half of them steepest descent, the other half conjugate gradient).

## ■ ASSOCIATED CONTENT

### Supporting Information

This material is available free of charge via the Internet at <http://pubs.acs.org>.

### Accession Codes

Coordinates and structure factors are available from the Protein Data Bank with accession codes 4B6O, 4B6P, 4B6Q, 4B6R, and 4B6S for DHQ2-Mt/4a, DHQ2-Mt/4c, DHQ2-Mt/5b, DHQ2-Hp/4a, and DHQ2-Hp/4c binary complexes, respectively.

## ■ AUTHOR INFORMATION

### Corresponding Author

\*E-mail: [concepcion.gonzalez.bello@usc.es](mailto:concepcion.gonzalez.bello@usc.es).

### Notes

The authors declare no competing financial interest.

## ■ ACKNOWLEDGMENTS

Financial support from the Xunta de Galicia (10PXIB2200122PR and GRC2010/12) and the Spanish Ministry of Science and Innovation (SAF2010-15076 to CGB and BFU2008-01588/BMC to M.J.vR.) is gratefully acknowledged. L.T., A.P., and V.F.V.P. thank the Spanish Ministry of Science and Innovation for FPU fellowships and the Portuguese Fundação para a Ciência e a Tecnologia for an FCT fellowship, respectively. J.M.O. thanks the Xunta de Galicia and Spanish Ministry of Science and Innovation for “Ángeles Alvario” and “José Castillejo” fellowships, respectively. We are also grateful to the ESRF and Soleil Synchrotron for measuring time on beamline ID14-1 and Proxima 1, respectively, and Andrew Thompson for his technical assistance with X-ray measurements. We are also grateful to the Centro de Supercomputación de Galicia (CESGA) for use of the Finis Terrae computer.

## ■ REFERENCES

- (1) For a data base of essential bacterial genes see: [www.essentialgene.org](http://www.essentialgene.org).
- (2) Zhang, R., and Lin, Y. (2009) DEG 5.0, a database of essential genes in both prokaryotes and eukaryotes. *Nucleic Acids Res.* 37, D455–D458.
- (3) Kleanthous, C. K., Deka, R., Davis, K., Kelly, S. M., Cooper, A., Harding, S. E., Price, N. C., Hawkins, A. R., and Coggins, J. R. (1992)

A comparison of the enzymological and biophysical properties of two distinct classes of dehydroquinase enzymes. *Biochem. J.* 282, 687–695.

- (4) Gourley, D. G., Shrive, A. K., Polikarpov, I., Krell, T., Coggins, J. R., Hawkins, A. R., Isaacs, N. W., and Sawyer, L. (1999) The two types of 3-dehydroquinase have distinct structures but catalyse the same overall reaction. *Nat. Struct. Biol.* 6, 521–525.

- (5) Harris, J., González-Bello, C., Kleanthous, C., Coggins, J. R., Hawkins, A. R., and Abell, C. (1996) Evidence from kinetic isotope studies for an enolate intermediate in the mechanism of type II dehydroquinases. *Biochem. J.* 319, 333–336.

- (6) Roszak, A. W., Robinson, D. A., Krell, T., Hunter, I. S., Frederickson, M., Abell, C., Coggins, J. R., and Laphorn, A. J. (2002) The structure and mechanism of the type II dehydroquinase from *Streptomyces coelicolor*. *Structure* 10, 493–503.

- (7) Krell, T., Pitt, A. R., and Coggins, J. R. (1995) The use of electrospray mass spectrometry to identify an essential arginine residue in type II dehydroquinases. *FEBS Lett.* 360, 93–96.

- (8) Krell, T., Horsburgh, M. J., Cooper, A., Kelly, S. M., and Coggins, J. R. (1996) Localization of the active site of type II dehydroquinase. Identification of a common arginine-containing motif in the two classes of dehydroquinases. *J. Biol. Chem.* 271, 24492–24497.

- (9) Prazeres, V. F. V., Castedo, L., Lamb, H., Hawkins, A. R., and González-Bello, C. (2009) 2-Substituted-3-dehydroquinic acids as potent competitive inhibitors of type II dehydroquinase. *ChemMedChem* 4, 1980–1984.

- (10) Peón, A., Otero, J. M., Tizón, L., Prazeres, V. F. V., Llamas-Saiz, A. L., Fox, G. C., van Raaij, M. J., Lamb, H., Hawkins, A. R., Gago, F., Castedo, L., and González-Bello, C. (2010) Understanding the key factors that control the inhibition of type II dehydroquinase by (2R)-2-benzyl-3-dehydroquinic acids. *ChemMedChem* 5, 1726–1733.

- (11) Robinson, D. A., Stewart, K. A., Price, N. C., Chalk, P. A., Coggins, J. R., and Laphorn, A. J. (2006) Crystal structures of *Helicobacter pylori* type II dehydroquinase inhibitor complexes: new directions for inhibitor design. *J. Med. Chem.* 49, 1282–1290.

- (12) The X-ray crystal structure is available from the Protein Data Bank (PDB code: 1H0S): Robinson, D. A., Roszak, A. W., Frederickson, M., Abell, C., Coggins, J. R., and Laphorn, A. J. Structural basis for specificity of oxime based inhibitors towards type II dehydroquinase from *M. tuberculosis*, unpublished material. Residues 20–25 are not visible, including the essential residue Tyr24.

- (13) Dias, M. V. B., Snee, W. C., Bromfield, K. M., Payne, R. J., Palaninathan, S. K., Ciulli, A., Howard, N. I., Abell, C., Sacchettini, J. C., and Blundell, T. L. (2011) Structural investigation of inhibitor designs targeting 3-dehydroquinase dehydratase from the shikimate pathway of *Mycobacterium tuberculosis*. *Biochem. J.* 436, 729–739.

- (14) Finzel, B. C., Baldwin, E. T., Bryant, G. L., Hess, G. F., Wilks, J. W., Trepod, C. M., Mott, J. E., Marshall, V. P., Petsold, G. L., Poorman, R. A., Ósullivan, T. J., Schostarez, H. J., and Mitchell, M. A. (1998) Structural characterizations of nonpeptidic thiazolidine inhibitors of matrix metalloproteinases reveal the basis for stromelysin selectivity. *Protein Sci.* 7, 2118–2126.

- (15) Mortenson, D. E., Satyshur, K. A., Guzei, I. A., Forest, K. T., and Gellman, S. H. (2012) Quasiracemic crystallization as a tool to assess the accommodation of noncanonical residues in nativelike protein conformations. *J. Am. Chem. Soc.* 134, 2473–2476.

- (16) Cornilescu, G., Hadley, E. B., Woll, M. G., Markley, J. L., Gellman, S. H., and Cornilescu, C. C. (1997) Solution structure of a small protein containing a fluorinated side chain in the core. *Protein Sci.* 16, 14–19.

- (17) Blanco, B., Sedes, A., Peón, A., Lamb, H., Hawkins, A. R., Castedo, L., and González-Bello, C. (2012) Synthesis of 3-alkyl enol mimics inhibitors of type II dehydroquinase: factors influencing their inhibition potency. *Org. Biomol. Chem.* 10, 3662–3676.

- (18) Prazeres, V. F. V., Sánchez-Sixto, C., Castedo, L., Shuh, S. W., Lamb, H., Hawkins, A. R., Cañada, F. J., Jiménez-Barbero, J., and González-Bello, C. (2008) Competitive inhibitors of *Helicobacter pylori* type II dehydroquinase: synthesis, biological evaluation, and NMR studies. *ChemMedChem* 3, 756–770.

- (19) Gourley, D. G., Coggins, J. R., Isaacs, N. W., Moore, J. D., Charles, I. G., and Hawkins, A. R. (1994) Crystallization of a type II dehydroquinase from *Mycobacterium tuberculosis*. *J. Mol. Biol.* **241**, 488–491.
- (20) Leslie, A. G. (2006) The integration of macromolecular diffraction data. *Acta Crystallogr., Sect. D* **62**, 48–57.
- (21) Evans, P. (2006) Scaling and assessment of data quality. *Acta Crystallogr., Sect. D* **62**, 72–82.
- (22) Winn, M. D. (2003) An overview of the CCP4 project in protein crystallography: an example of a collaborative project. *J. Synchrotron Radiat.* **10**, 23–25.
- (23) McCoy, A. J., Grosse-Kunstleve, R. W., Adams, P. D., Winn, M. D., Storoni, L. C., and Read, R. J. (2007) J. Phaser crystallographic software. *Appl. Cryst.* **40**, 658–674.
- (24) Schüttelkopf, A. W., and van Aalten, D. M. F. (2004) PRODRG: a tool for high-throughput crystallography of protein-ligand complexes. *Acta Crystallogr. D60*, 1355–1363.
- (25) Emsley, P., and Cowtan, K. (2004) Coot: model-building tools for molecular graphics. *Acta Crystallogr., Sect. D* **60**, 2126–2132.
- (26) Brünger, A. T. (1997) Free R value: cross-validation in crystallography. *Methods Enzymol.* **277**, 366–396.
- (27) Murshudov, G. N., Vagin, A. A., and Dodson, E. J. (1997) Refinement of macromolecular structures by the maximum-likelihood method. *Acta Crystallogr., Sect. D* **53**, 240–255.
- (28) Davis, I. W., Leaver-Fay, A., Chen, V. B., Block, J. N., Kapral, G. J., Wang, X., Murray, L. W., Arendall, W. B., 3rd, Snoeyink, J., Richardson, J. S., and Richardson, D. C. (2007) MolProbity: all-atom contacts and structure validation for proteins and nucleic acids. *Nucleic Acids Res.* **35**, W375–W383.
- (29) DeLano, W. L. (2008) The PyMOL Molecular Graphics System. DeLano Scientific LLC, Palo Alto, CA. <http://www.pymol.org>.
- (30) Frisch, M. J., Trucks, G. W., Schlegel, H. B., Scuseria, G. E., Robb, M. A., Cheeseman, J. R., Scalmani, G., Barone, V., Mennucci, B., Petersson, G. A., Nakatsuji, H., Caricato, M., Li, X., Hratchian, H. P., Izmaylov, A. F., Bloino, J., Zheng, G., Sonnenberg, J. L., Hada, M., Ehara, M., Toyota, K., Fukuda, R., Hasegawa, J., Ishida, M., Nakajima, T., Honda, Y., Kitao, O., Nakai, H., Vreven, T., Montgomery, Jr., J. A., Peralta, J. E., Ogliaro, F., Bearpark, M., Heyd, J. J., Brothers, E., Kudin, K. N., Staroverov, V. N., Kobayashi, R., Normand, J., Raghavachari, K., Rendell, A., Burant, J. C., Iyengar, S. S., Tomasi, J., Cossi, M., Rega, N., Millam, J. M., Klene, M., Knox, J. E., Cross, J. B., Bakken, V., Adamo, C., Jaramillo, J., Gomperts, R., Stratmann, R. E., Yazyev, O., Austin, A. J., Cammi, R., Pomelli, C., Ochterski, J. W., Martin, R. L., Morokuma, K., Zakrzewski, V. G., Voth, G. A., Salvador, P., Dannenberg, J. J., Dapprich, S., Daniels, A. D., Farkas, Ö., Foresman, J. B., Ortiz, J. V., Cioslowski, J., and Fox, D. J. (2009) *Gaussian 09, Revision A.2*, Gaussian, Inc., Wallingford, CT.
- (31) Cornell, W. D., Cieplak, P., Bayly, C. I., Gould, I. R., Merz, K. M., Ferguson, D. M., Spellmeyer, D. C., Fox, T., Caldwell, J. W., and Kollman, P. A. (1995) A second generation force field for the simulation of proteins, nucleic acids, and organic molecules. *J. Am. Chem. Soc.* **117**, 5179–5197.
- (32) Case, D. A., Cheatham, T. E., Darden, T., Gohlke, H., Luo, R., Merz, K. M., Onufriev, O., Simmerling, C., Wang, B., and Woods, R. J. (2005) The Amber biomolecular simulation program. *J. Comput. Chem.* **26**, 1668–1688.
- (33) Wang, J., Wang, W., Kollman, P. A., and Case, D. A. (2006) Automatic atom type and bond type perception in molecular mechanical calculations. *J. Mol. Graphics Modell.* **25**, 247–260.
- (34) Price, N. C., Boam, D. J., Kelly, S. M., Duncan, D., Krell, T., Gourley, D. G., Coggins, J. R., Virden, V., and Hawkins, A. R. (1999) The folding and assembly of the dodecameric type II dehydroquinases. *Biochem. J.* **338**, 195–202.
- (35) Li, H., Robertson, A. D., and Jensen, J. H. (2005) Very fast empirical prediction and rationalization of protein pKa values. *Proteins* **61**, 704–721.
- (36) Bas, D. C., Rogers, D. M., and Jensen, J. H. (2008) Very fast prediction and rationalization of pKa values for protein–ligand complexes. *Proteins* **73**, 765–783.
- (37) Olsson, M. H. M., Søndergard, C. R., Rostkowski, M., and Jensen, J. H. (2011) PROPKA3: consistent treatment of internal and surface residues in empirical pKa predictions. *J. Chem. Theor. Comp.* **7**, 525–537.
- (38) Søndergard, C. R., Olsson, M. H. M., Rostkowski, M., and Jensen, J. H. (2011) Improved treatment of ligands and coupling effects in empirical calculation and rationalization of pKa values. *J. Chem. Theor. Comp.* **7**, 2284–2295.
- (39) Case, D. A., Darden, T. A., Cheatham III, T. E., Simmerling, C. L., Wang, J., Duke, R. E., Luo, R., Walker, R. C., Zhang, W., Merz, K. M., Roberts, B., Wang, B., Hayik, S., Roitberg, A., Seabra, G., Kolossvai, I., Wong, K. F., Paesani, F., Vanicek, J., Liu, J., Wu, X., Brozell, S. R., Steinbrecher, T., Gohlke, H., Cai, Q., Ye, X., Wang, J., Hsieh, M.-J., Cui, G., Roe, D. R., Mathews, D. H., Seetin, M. G., Sagui, C., Babin, V., Luchko, T., Gusarov, S., Kovalenko, A., and Kollman, P. A. (2010) *Amber Tools 1.5*, AMBER 11, University of California, San Francisco, CA.
- (40) Aqvist, J. (1990) Ion-water interaction potentials derived from free energy perturbation simulations. *J. Phys. Chem.* **94**, 8021–8024.
- (41) Jorgensen, W. L., Chandrasekhar, J., and Madura, J. D. (1983) Temperature and size dependence for Monte Carlo simulations of TIP4P water. *J. Chem. Phys.* **79**, 926–935.
- (42) Darden, T. A., York, D., and Pedersen, L. G. (1993) Particle mesh Ewald: An  $W \log(N)$  method for Ewald sums in large systems. *J. Chem. Phys.* **98**, 10089–10092.
- (43) Ryckaert, J.-P., Ciccotti, G., and Berendsen, H. J. C. (1977) Numerical integration of the cartesian equations of motion of a system with constraints: molecular dynamics of n-alkanes. *J. Comput. Phys.* **23**, 327–341.